Applied Thermal Engineering 229 (2023) 120470

Contents lists available at ScienceDirect

Applied Thermal Engineering

journal homepage: www.elsevier.com/locate/apthermeng

Research Paper

Impingement jets on a confined assembly of rotating hot cylinder covered by a surface porous layer

Muneer A. Ismael [a,b,*], Obai Younes [c,d], Mehdi Fteiti [e], Mohammad Ghalambaz [f], Raad Z. Homod [g]

[a] Mechanical Engineering Department, Engineering College, University of Basrah, Basra, Iraq
[b] College of Engineering, University of Warith Al-Anbiyaa, Karbala, Iraq
[c] Department of Mechanical Engineering, College of Engineering in Wadi Addwasir, Prince Sattam Bin Abdulaziz University, Al-Kharj 11942, Saudi Arabia
[d] Department of Mechanical Engineering, Faculty of Engineering, University of Khartoum, Sudan
[e] Physics Department, Faculty of Applied Science, Umm Al-Qura University, Makkah 24381, Saudi Arabia
[f] Laboratory on Convective Heat and Mass Transfer, Tomsk State University, 634045 Tomsk, Russia
[g] Department of Oil and Gas Engineering, Basrah University for Oil and Gas, Basra, Iraq

ARTICLE INFO

Keywords:
Impingement jets
Porous surface layer
Rotating cylinder
Eccentricity
Temperature uniformity

ABSTRACT

Thermal stresses encountered in the production of steel rod is a challenging problem arising from the irregular temperature distribution along the circumference of the rod. This study investigates the cooling process of a hot cylinder with a uniform surface temperature. The concept of the problem is a rotating cylinder immersed in an annular porous medium under the impact of two impinging jets. The jets are confined and act upward and downward. The rotational speed of the cylinder, the eccentricity of the surface porous layer and its Darcy number and Reynolds number are varied to organize the feasibility of the suggested problem. The parameters are controlled to be within the laminar mathematical system, which is solved computationally using the finite element method. The results show a promising role of the porous surface layer as it raises the Nusselt number, where it elevates 78% greater than a bared cylinder for a Darcy number $Da = 10^{-2}$ and a Reynolds number $Re = 400$. It was found that although the rotation of the cylinder reduces the Nusselt number, it contributes highly to the uniformity of the surface temperature of the cylinder. It was found also that the eccentricity of the porous layer increases the average Nusselt number by 28% for $Re = 300$ and $Da = 10^{-2}$. The porous layer and the cylinder rotation increase slightly the pressure drop.

1. Introduction

The metallurgists strictly recommend a uniform surface temperature of hot steel during the continuous heat treatment. Thus, the production of steel needs special efforts in optimizing the cooling process because of its low thermal diffusivity [1]. The uniform surface temperature ensures the uniformity of the temperature throughout the entire steel product [2], which in turn reduces the possibility of forming thermal stresses. Other examples of uniform temperature demands are encountered in cooling the turbine shaft [3] and cooling a work-piece under a grinding process [4]. Impinging jet spraying water drops on the hot surface is one of the diversities technical methods followed in ensuring uniform cooling of continuous heat treatment of heated products. Despite the temperature uniformity of hot cylinders being the main demand in heat treatment, but the augmentation of convective heat transfer is also one of the most important requirements. In the late 1980′s, some experimental works arose to boost the convective heat transfer from hot bodies by embedding them in a layer of a porous medium. Nasr et al. [5] cited most of these works and endorsed their results by experiments on cross-flow over a hot cylinder embedded in diverse porous media. They employed different solid matrices by changing the type and size of spheres forming the porous media and proposed smaller sizes and higher thermal conductivity to get a heat transfer coefficient seven times greater than bared cylinder exposed to the same cross-flow. Layeghi and Nouri-Borujerdi [6] performed a parametric numerical study to show the augmentation of the heat transfer of a heated cylinder embedded in a Darcian porous medium and subjected to low Reynolds numbers flow.

* Corresponding Author.
E-mail addresses: muneer.ismael@uobasrah.edu.iq (M.A. Ismael), oubeytaha@hotmail.com (O. Younes), mafteiti@uqu.edu.sa (M. Fteiti), m.ghalambaz@gmail.com (M. Ghalambaz), raad@buog.edu.iq, raadahmood@yahoo.com (R.Z. Homod).

https://doi.org/10.1016/j.applthermaleng.2023.120470
Received 5 September 2022; Received in revised form 22 February 2023; Accepted 22 March 2023
Available online 25 March 2023

Nomenclature

C_f	Friction coefficient of Forchheimer term
d	Diameter of the annular porous layer (m)
D	Diameter of the cylinder (m)
Da	Darcy number ($K.D^{-2}$)
H	Height of the channel
K	Permeability (m^2)
k	Thermal conductivity ($W.m^{-1}.K^{-1}$)
Kr	Conductivity ratio (k_{eff}/k_f)
L	Length of the channel (m)
Nu	Nusselt number, local
n	Normal vector
P	Pressure ($N.m^{-2}$)
Pe	Peclet number (Re*Pr)
Pr	Prandtl number (ϑ/α)
q“	Heat flux ($W.m^{-2}$)
Re	Reynolds number ($\rho V_{in} D/\mu$)
S	Distance along the cylinder (m)
U	Velocity vector
U,V	Velocities, dimensionless
u, v	Velocities, dimensional ($m.s^{-1}$)
u, v	Velocities ($m.s^{-1}$)
Vin	Jet velocity ($m.s^{-1}$)
W	Width of slot jet (m)
X,Y	Dimensionless Cartesian coordinates
x, y	Cartesian coordinates (m)

Greek Symbols

α	Thermal diffusivity ($m.s^{-2}$)
δ	Eccentricity (m)
ε	porosity
λ	Switching parameter
μ	Dynamic viscosity ($kg.m^{-1}.s^{-1}$)
ρ	Density ($kg.m^{-3}$)
Ψ	Streamfunction, dimensionless
Ω	Rotational speed, dimensionless

Subscripts

av	average
C	cold
eff	effective
f	Fluid
p	porous

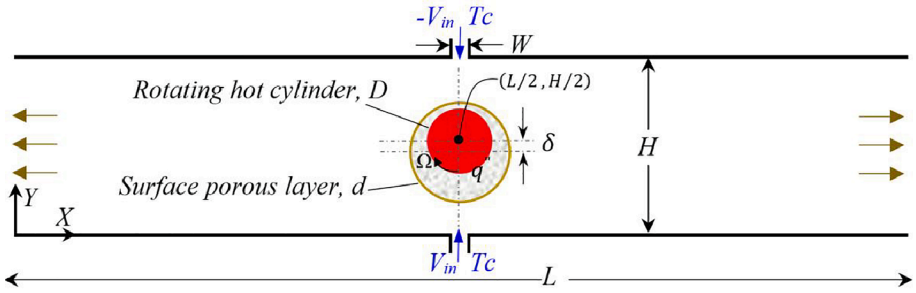

Fig. 1. Schematic illustration of the problem.

Table 1
Test of numerical solution dependence against the size of mesh for Re = 400, Ω = 15, Da = 10^{-2}, δ/D = 0.15.

Mesh	Mesh size	Average Nusselt number	Percentage error
M1	13,874	4.4165	–
M2	25,464	5.1686	14.5
M3	59,518	6.5078	20.5
M4	141,118	6.9006	5.7
M5	269,658	6.9187	0.26

They did not focus their attention on the existence of the porous medium, but they indicated lower porosity in order to get a higher Nusselt number. Al-Sumaily et al. [7] extended the conditions of Layeghi and Nouri-Borujerdi [6] by considering higher Nusselt numbers (up to 250) and so that non-Darcian model became mandatory to be used. Moreover, their study was unsteady and took into consideration the local thermal non-equilibrium LTNE between the solid matrix of the porous medium and the entrained fluid. They invoked two roles of the porous medium, the first is the augmentation of the Nusselt number, and the second is the elimination of the separation flow along the hot cylinder. The LTNE model has resulted in a different key parameter governing the Nusselt number in the fluid phase. Sayehvand et al. [8] extended the problem of Al-Sumaily et al. [7] by embedding a pair of cylinders in a horizontal channel saturated with a porous medium. They endorsed the enhancement of heat transfer due to the presence of the porous medium and attributed this enhancement to the wake region behind the cylinders as in the clear channel. However, the drawback of the porous medium is the increase in the total pressure drop. The horizontal distance between the two cylinders was a strong parameter affecting the heat released from the cylinders. The experiments of Al-Salem et al. [9] on a heated cylinder wrapped by a porous annular sheet and subjected to cross-flow have recorded a positive role of the annular porous sheet in augmenting the Nusselt number. According to their findings, the pressure drop arising from the porous layer is not so considerable, while its thickness should not be too high in order to avoid air trapping within it. In the same topic, Rashidi et al. [10] inspected two types of spheres forming a porous ring surrounding a hot cylinder and subjected to a low flow of water. Relative to the thermal conductivity of the cooling fluid (water), the spheres of higher thermal conductivity gave a higher Nusselt number than the spheres of lower thermal conductivity. The length of the wake extended with decreasing the Darcy number. They proposed a porous medium of high thermal conductivity and high permeability for perfect heat transfer. Tumes et al. [11] investigated the role of the magnetic field and the ferrofluid volume fraction on the hydrodynamic, thermodynamic and thermal behaviors of a cylindrical body subjected to a stream of water-Fe_3O_4 ferrofluid inside a horizontal channel. They reported that the magnetic field augments the Nusselt number and reduces the entropy generation. Howsoever, their proposed parameters that give optimum performance implied to zero magnetic field and 4% volume

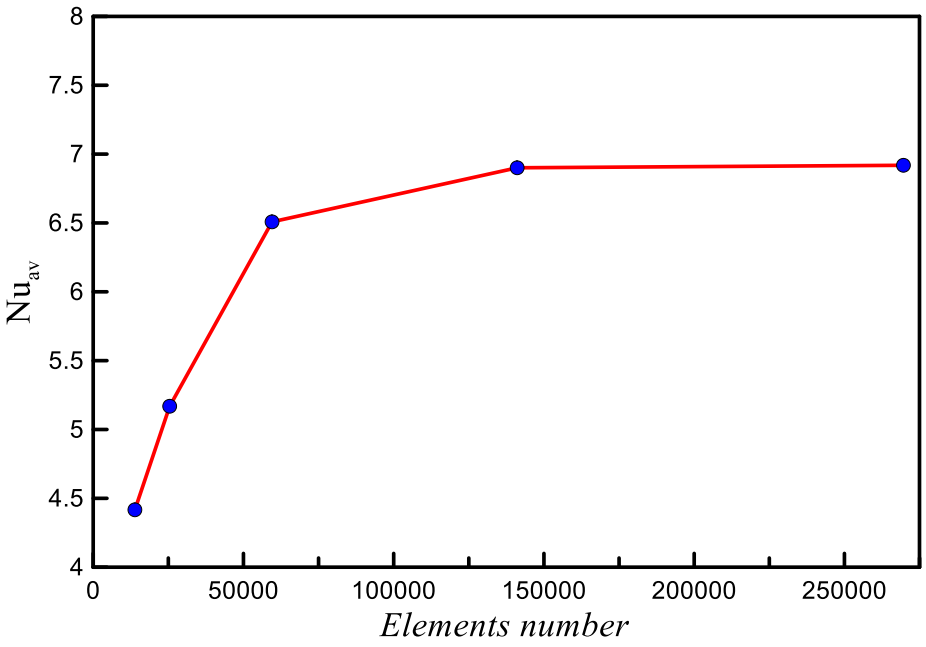

Fig. 2. Test of numerical solution dependence against the size of mesh for Re = 400, Ω = 15, Da = 10^{-2} and δ/D = 0.15.

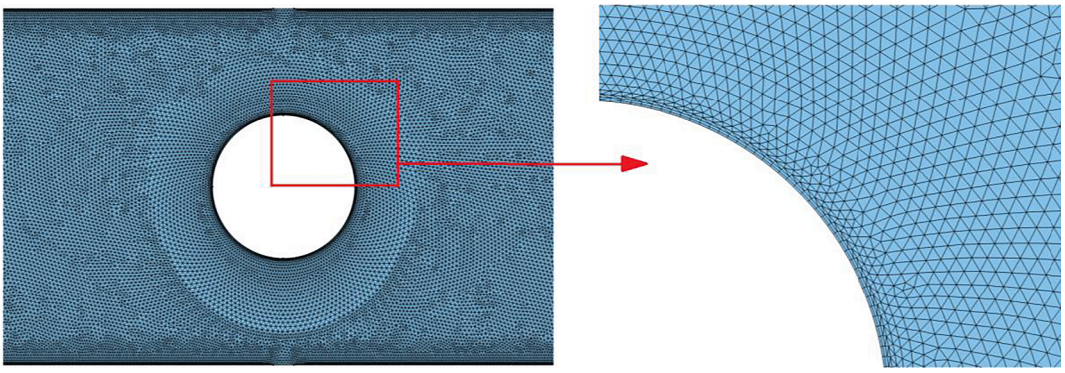

Fig. 3. Mesh topography of G4 (141118 elements) for Re = 400, Ω = 15, Da = 10^{-2}, δ/D = 0.15.

Table 2
Comparison of the average Nusselt number along the cylinder between the present numerical solution and experimental results of Nasr et al. [5] and numerical solution of Al-Sumaily [47].

Pe	Experimental, Nasr et al. [5]	Numerical, Al-Sumaily [47]	Present-constant heat flux	$\%Error = \frac{\lvert Nu_{Present} - Nu_{[3]} \rvert}{Nu_{[5]}}$
103	11.56	13.16	13.645	18
120	12.30	14.42	14.266	16
125	12.80	14.90	14.480	13
139	14.00	15.56	14.991	7
150	14.88	16.54	15.350	3.2
181	16.07	18.40	16.447	2.3
192	17.34	19.11	16.830	3
201	17.75	19.70	17.140	3.5
211	18.58	–	17.480	6

fraction of the ferrofluid.

Covering bluff bodies by a porous ring has been investigated deeply in the field of aerodynamics. This is because the porous layer plays a major role in controlling the length of the wake, the formation of the vortex shedding and hence, the acoustic noise in environmental applications. Moreover, the passive nature of this strategy has attracted the attention of researchers on this topic. A common conclusion among most works is that the porous cover layer regularizes the fluctuations in the velocity and pressures behind the bluff bodies (Naito and Fukagata [12]), and this action is more pronounced in circular than rectangular bluff bodies (Sadeghipour et al. [13]). The porous layer reduces the drag in the covered square bluff body and inversely increases the drag in the case of circular cylinders (Showkat et al. [14]). A very interesting role of the porous layer is the coating of linkage arms used in the mechanism of obtaining the electricity from the mains to drive the high-speed train (Liu et al. [15]); this is a very important demand in reducing the noise raised from the strong turbulence around the linkages cylindrical arms.

To enhance the heat removal from an object, a controllable flow direction can be achieved by applying an impingement jet to carry the coolant on that object (Farzad et al. [16]). When the object is a porous block of different geometries placed on a heat source, Fu and Huang [17] recommended the concave geometry to achieve higher spacing between the jet and the porous block. Chen and Cheng [18] suggested double concave porous layers covering a curved grove made on a copper block. The concave bilayer is subjected to a nanofluid impingement jet. To get more heat transfer, they advised that the porosity of the upper layer should be higher than that of the lower layer. The study of Fischer and Lemos [19] revealed that the jet impinging on a heated plate covered by

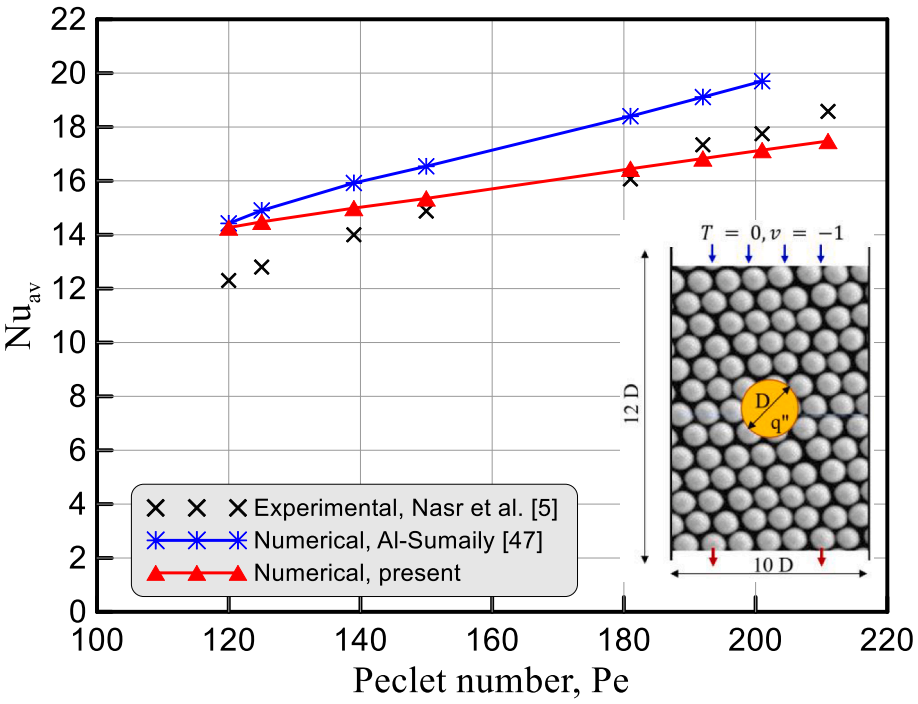

Fig. 4. Comparison between the outcomes of the present solution with experimental results of Nasr et al. [5] and numerical results of Al-Sumaily [47].

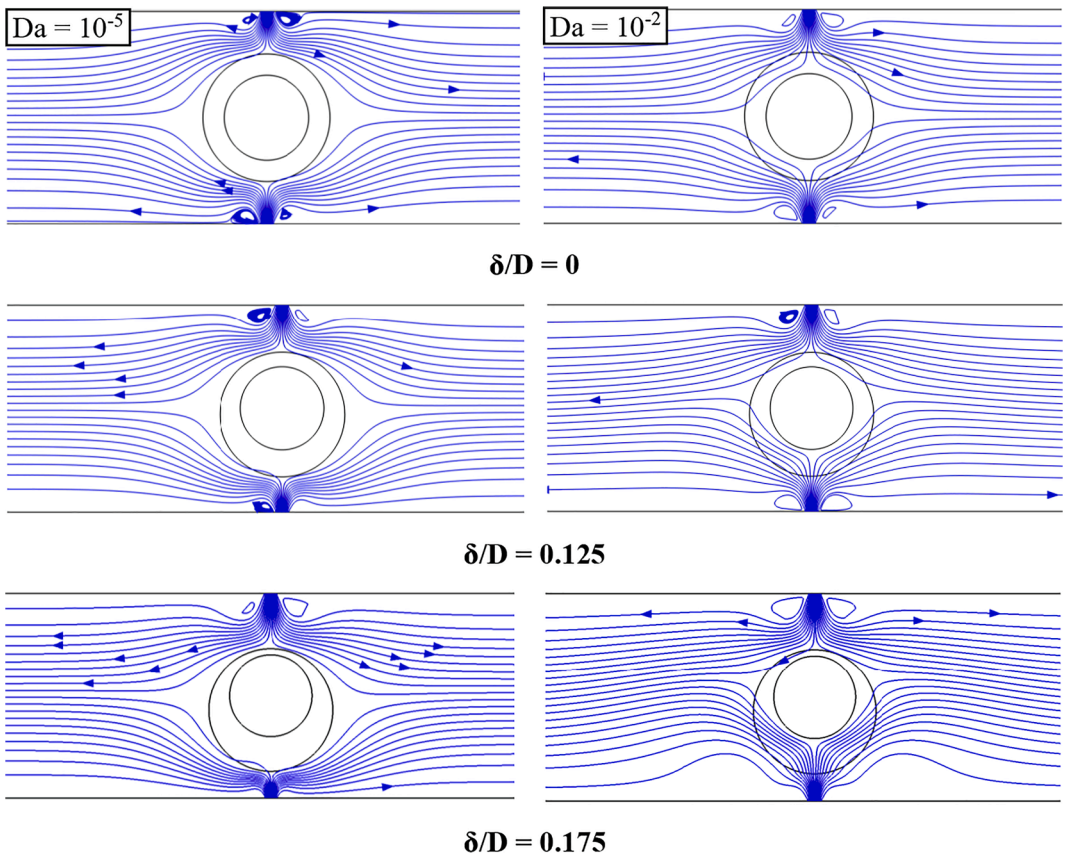

Fig. 5. Streamlines around still cylinder (Ω = 0) for three different eccentricities and Re = 300.

a porous layer not only enhances the heat removal but also suppresses the Nusselt number's peaks at the stagnation region. Choo et al. [20] proved experimentally the benefit of inclining the impingement of jet on the Nusselt number presuming the spacing between the jet and the hot plate is equal to or less than the nozzle diameter. Bentarzi et al. [21] assumed two jets impinging with different configurations; parallel (oblique and perpendicular), divergent and convergent. They indicated that no inclination configuration gave the Nusselt number more than the

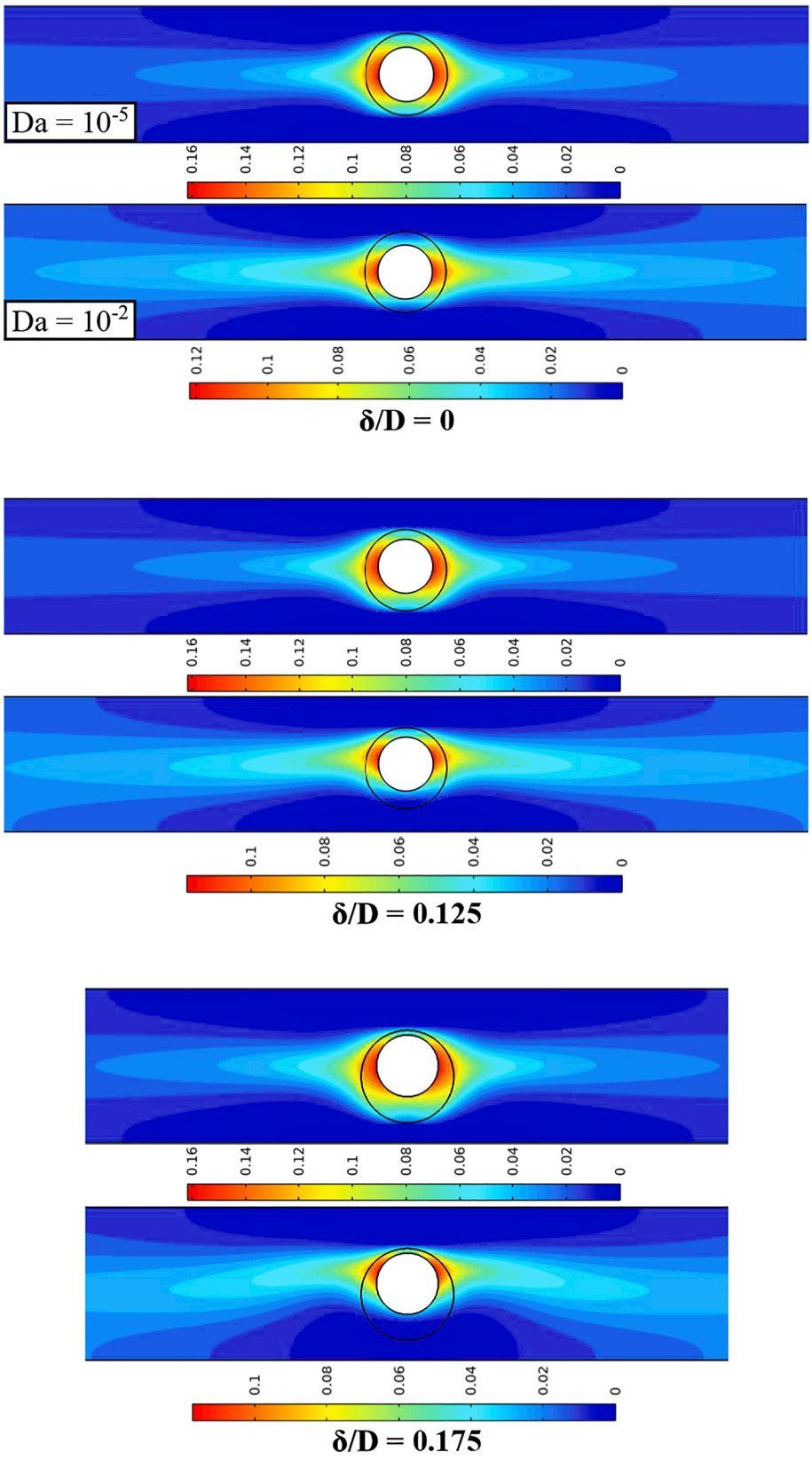

Fig. 6. Isotherms of stationary cylinder (Ω = 0) for three different eccentricities and Re = 300.

perpendicular jets. This was because they were not aware of the spacing between the jets and the hot wall, namely, they assumed a distance of eight times of jet width, which is so large that it causes losses of momentum of the wall jet [20]. Besides the benefit of inclining the jet of the heat transfer, Benmouhoub and Mataoui [22] inspected the effect of moving the hot wall also. Their findings showed that the movement of the hot wall is useful when its speed is greater than the jet velocity; otherwise, the movement of the wall decreases the Nusselt number.

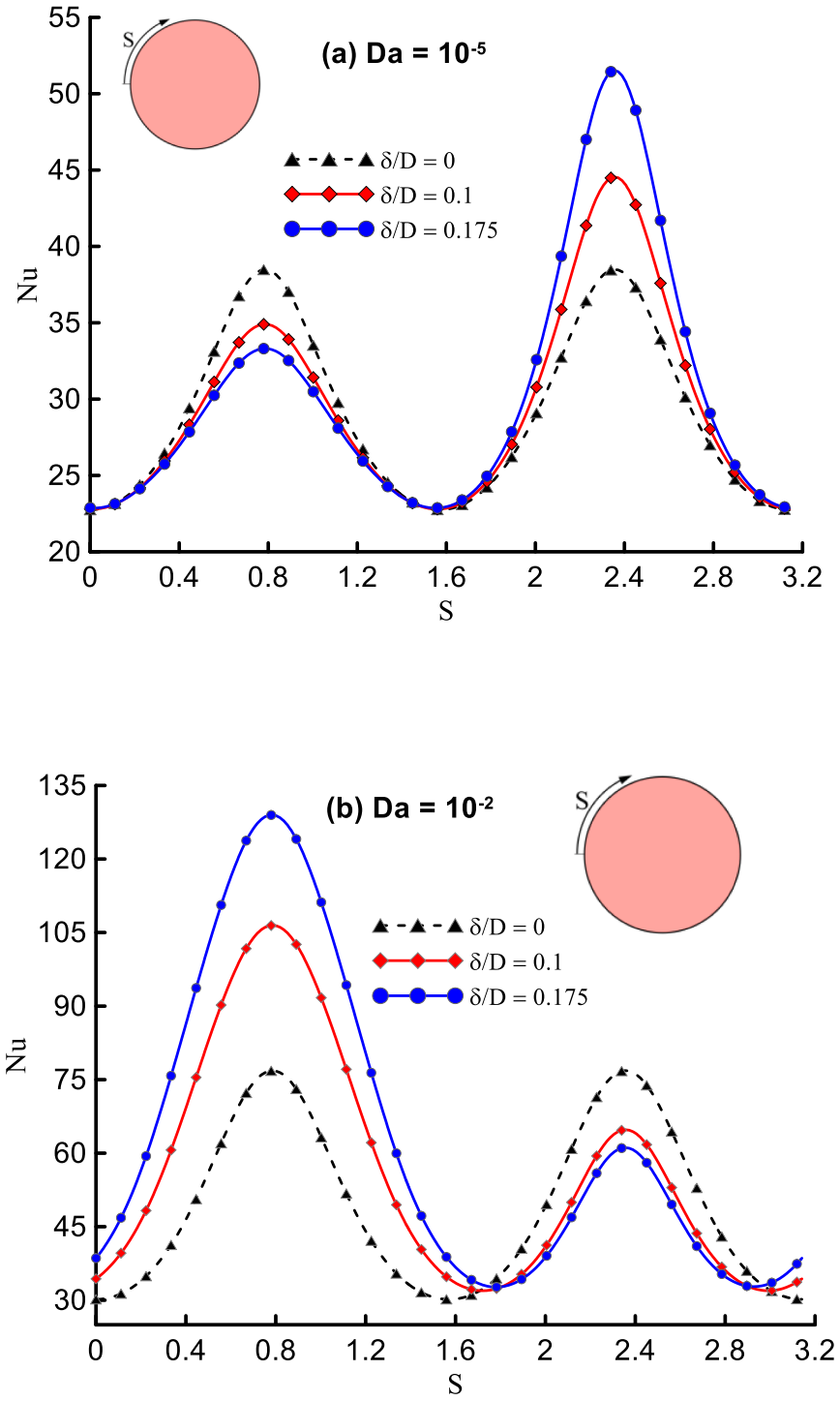

Fig. 7. Local Nusselt number for Re = 300, Ω = 0, and (a) Da = 10^{-5}, (b) Da = 10^{-2}.

Contrarily, Chattopadhyay and Saha [23] showed that the heat transfer from the knife or axial jets decreases with increasing the velocity of the hot surface. However, the knife jets showed better heat transfer from the axial jets when the surface velocity is about one-half the jet velocity. Sharma and Sahu [24] observed experimentally an increase and decrease of the heat flux with the Reynolds number of impinging jet and the speed the moving steel foil, respectively. Lai et al. [25] focused their experiments on the flow characteristics of an inclined jet impinging on a rotating disk. They proved a crucial role in the centrifugal force imparted by the rotating disk to the fluid, where the excessive rotational speed pushes the jet away from the target. Moreover, when the rotational Reynolds number is 38 times the jet Reynolds number, the flow is governed by rotation. Dutta and Chattopadhyay [26] studied the annular turbulent jet impinging upon a circular hot disc and presented significant details about the fluid circulation and its kinetic energy. They presented the prominent role of the Reynolds number on the shape and size of the reverse zone. Hosseinalipour et al. [27] used a local thermal non-equilibrium model to investigate laminar pulsed impinging jet in the existence of porous metallic blocks. They, first, evaluated the steady impinging jet on porous blocks, and then examined the impact of the porous blocks on the puled impingement jet. They also examined the impact of various pulse frequencies and amplitudes. They concluded

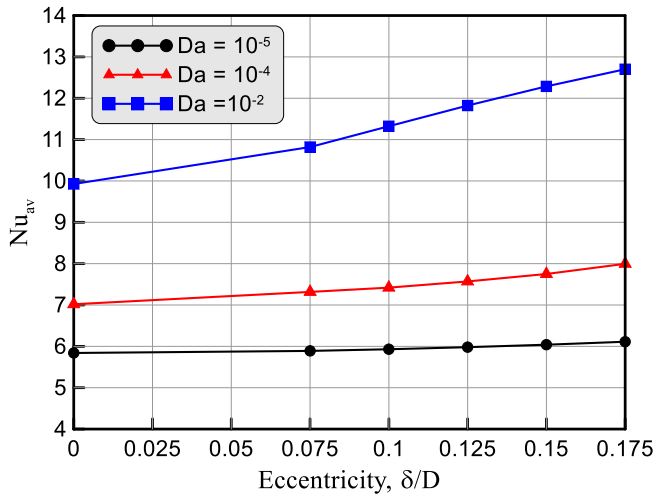

Fig. 8. Variation of Nusselt number with the eccentricities and different Darcy number for Re = 300 and Ω = 0.

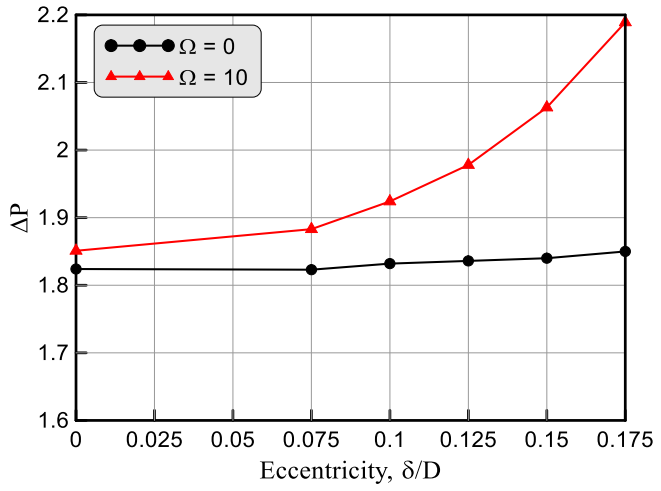

Fig. 9. Pressure drop with the eccentricity and the Rotational speed for Re = 100 and Da = $10^{-3.}$

that the Nusselt number was not affected by lower values of pulse frequencies and amplitudes, while the existence of porous blocks resulted in a more flat distribution of the Nusselt number.

Concerning the cylindrical target, there are two purposes of the impingement jet; the first is for cooling or heating, in which case the cylinder is stationary [28]. The second purpose is heat treatments such as quenching or annealing where the cylinder is rotating [29,30]. The rotation of the cylinder eliminates the extreme values of the local Nusselt number rising from the stagnation points. Nada [31] demonstrated experimentally the virtue of the multiple jets distributed along a line parallel to the axis of a hot cylinder resulting in a uniform Nusselt number better than a single slot jet extended along the same line. Singh et al. [32] revealed experimentally the benefit of confining a stationary hot cylinder, subjected to a circular air jet, by a bottom semi-circular plate. Where the gain of the average Nusselt number was found to be 17% greater than the unconfined cylinder, then they promoted their findings by numerical simulation to get an increase of 24% in the local Nusselt number when the confining plate is split to form a longitudinal vent. In another study, Singh et al. [33] utilized the concave confining plate in the case of double circular jets. In this case, the gain of the average Nusselt number due to the confining was 16%. However, the separation between the jets had a positive impact on the total average Nusselt number. Pachpute and Premachandran [34] compared the performance of cooling a hot cylinder by the impingement jet with and without upper confinement. Their numerical results stated that the effect of the confining is negligible when its length is six times greater than the cylinder diameter. Alizadeh et al. [35] examined the impact of transpiration, permeability and porosity on the flow field and thermal performance of an external impinging jet around a cylinder. It was found that non-uniform transpiration remarkably influenced the field and thermal performance, while the impact of permeability and porosity was negligible.

Regarding the heat treatment applications, the experiments of Jahedi and Moshfegh [36] of using a row of inline circular jets on quenching heat transfer of a hollow, rotating shaft showed that the rotational speed of the shaft significantly affected the quenching process. They detected that the high rotational speed reduces the contact time between the jets and the shaft, thus resulting in poor quenching, while the low speed provides not only efficient cooling but it also produces uniform heat transfer. Jeng et al. [37] utilized the infrared technique and smoke to visualize the flow around a rotating hot cylinder subjected to a planner slot jet. Their results endorsed the role of cylinder rotation in getting a uniform Nusselt number along the circumferential of the cylinder, and the increase of the jet based Reynolds number led to increase the Nusselt number for rotating and stationary cylinder, while the rotation based Reynolds number led to increase the Nusselt number in case of no flow from the jet. However, when a hot cylinder rotates with no impingement jet, the rotation here causes a non-uniform distribution of the local Nusselt number as indicated by Ma et al. [38]. Bijarchi et al. [39] suggested a swinging-like pendulum slot jet to perform uniform cooling of a hot flat surface. They indicated that their suggested strategy accomplishes the uniform cooling provided that the jet to target ratio is between 0.35 and 0.5. Li et al. [40] considered the scarfing defects of the steel slabs cooled by a multiple jets. They imposed an inclination to a large number of multi-jet impingement with long jet-to-target spacing and investigated the problem numerically and visualized the flow fields experimentally. According to their results, Coanda effect was the main cause that triggers grooves on the slab, thus, the obliquely impingement parallel jets, spacing between them and the spacing between jets and the target were the key parameters that inspected to limit such a problem.

In summary, the use of impingement jets in cooling or heat-treating of circular cylinders or shafts is a viable strategy. Most studies have focused on the cooling of hot surfaces, and few studies addressed the homogenizing of the surface temperature. However, there is no individual work, to the best of our knowledge, which has focused on enhancing and getting uniform heat transfer of a heated cylinder. Moreover, impingement jets applied to a cylinder wrapped by a porous layer are not widely known and still need more understanding. Therefore, the aim of this paper is to introduce an approach to enhancing the cooling rate of a hot cylinder with uniform distribution of its surface temperature. The proposed approach is to cover the cylinder with an eccentric porous surface layer and apply two jets, upward and downward, with possible rotation of the cylinder. It is believed that this approach will contribute to new promising findings in heat treatment, which is an essential stage in the production of steel shafts.

2. Description of the model

The schematic diagram of Fig. 1 shows a hot cylinder of diameter D rotates with angular speed Ω and covered by an annular porous layer of outer diameter d. There is an eccentricity between the centers of the cylinder and the porous layer, assigned by δ. The covered cylinder is confined inside a horizontal channel of length L and height H. Two jets spout from the walls of the channel and impinge cold water upward and downward onto the covered cylinder. The width of each jet is W. Based on the cylinder diameter, the dimensions of the geometry are set as; $d/D = 1.5$, $H/D = 2.5$, $W/D = 0.15$ and $L/D = 30$. All dimensions are selected arbitrarily, except the channel length (L/D) and jet to target ratio (W/D).

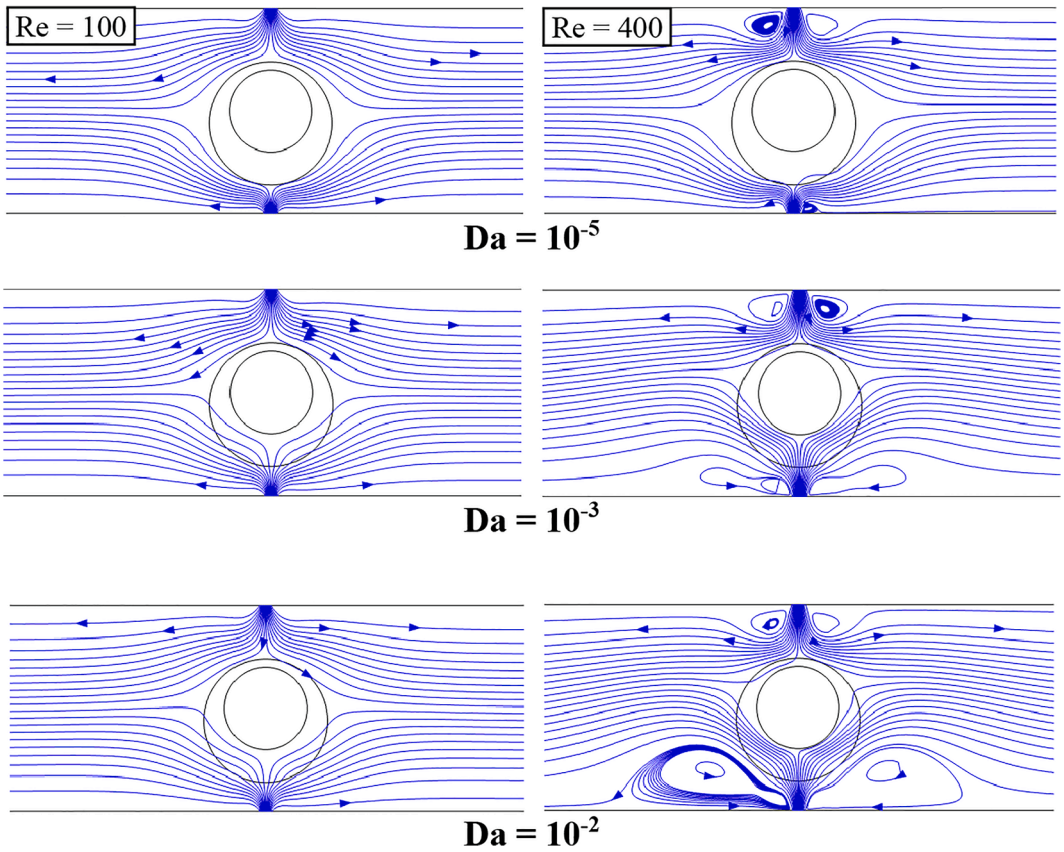

Fig. 10. Streamlines around stationary cylinder (Ω = 0) with Darcy number for Re = 100, 400 and δ/D = 0.15.

The L/D is selected to provide the condition of the fully developed flow at the two outlets of the cross-flow, where the value 30 is suitable for Reynolds number up to 500 according to the constraint $L/D = 0.06Re$. The W/D is adjusted to meet the affective distance between the jet opening and the target, which is the horizontal peaks of the rotating cylinder [41]. Considering an incompressible Newtonian fluid, steady laminar flow, and assuming too long a cylinder along with the slot jets, the variations in the thermal and flow fields in the direction normal to the X-Y plane are marginal and can safely be ignored. Owing to the strong inertia of the two jets, the buoyancy effect is ignored. Within the annular porous layer, the viscous and drag effects are taken into consideration by adopting the Darcy-Forchheimer model. Thus, the problem can be posed in terms of the following dimensionless equations.

$$\frac{\partial U}{\partial X}+\frac{\partial V}{\partial Y}=0 \tag{1}$$

$$\left(U\frac{\partial U}{\partial X}+V\frac{\partial U}{\partial Y}\right)=-\varepsilon^2\frac{\partial P}{\partial X}+\frac{\varepsilon}{Re}\left(\frac{\partial^2 U}{\partial X^2}+\frac{\partial^2 U}{\partial Y^2}\right)-\lambda\varepsilon^2\left(\frac{1}{ReDa}U+\frac{C_f}{\sqrt{Da}}|\mathbf{U}|U\right) \tag{2}$$

$$\left(U\frac{\partial V}{\partial X}+V\frac{\partial V}{\partial Y}\right)=-\varepsilon^2\frac{\partial P}{\partial Y}+\frac{\varepsilon}{Re}\left(\frac{\partial^2 V}{\partial X^2}+\frac{\partial^2 V}{\partial Y^2}\right)-\lambda\varepsilon^2\left(\frac{1}{ReDa}V+\frac{C_f}{\sqrt{Da}}|\mathbf{U}|V\right) \tag{3}$$

$$U\frac{\partial\theta}{\partial X}+V\frac{\partial\theta}{\partial Y}=\frac{(1+\lambda(Kr-1))}{RePr}\left(\frac{\partial^2\theta}{\partial X^2}+\frac{\partial^2\theta}{\partial Y^2}\right) \tag{4}$$

The value of λ is switched between 1 for the porous annular region and 0 for the remainder domain filled only with fluid. The equations above are derived from the original dimensional equations with the aid of the following parameters.

$$(U,V)=\frac{(u,v)}{V_{in}},\ P=\frac{p}{\rho V_{in}^2},\ \theta=\frac{(T-T_c)}{q''D/k_f},\ (X,Y)=\frac{(x,y)}{D}\ Re=\frac{\rho V_{in}D}{\mu},\ Pr=\frac{\mu}{\rho\alpha},\ Da=\frac{K}{D^2},\ Kr=\frac{k_{eff}}{k_f}$$

The term C_f in equations (2) an 3 is given by [42];

$$C_f=\frac{1.75}{\sqrt{150\varepsilon^3}} \tag{5}$$

where ε is the porosity.

The equivalent thermal conductivity in the porous region is given by:

$$k_{eff}=k_s(1-\varepsilon)+\varepsilon k_f \tag{6}$$

At the surface of the outer porous annular layer, the interface is represented by: $U,V,\theta|_f = U,V,\theta|_p$,$\left(\frac{\partial U}{\partial Y}+\frac{\partial V}{\partial X}\right)_f=\left(\frac{\partial U}{\partial Y}+\frac{\partial V}{\partial X}\right)_p$ and $k_f\frac{\partial\theta}{\partial Y}\Big|_f = .k_{eff}\frac{\partial\theta}{\partial y}\Big|_p$

The boundary conditions are as follows:

1) At the jets, $\theta = U = 0$, and $V = +1$ for the upward jet and $V = -1$ for the downward jet.

2) At the outlets of the cross-flow, $P = 0, \partial U/\partial X = \partial V/\partial X = \partial\theta/\partial X = 0$

3) At the surface of the cylinder, $\frac{\partial\theta}{\partial n} = -1$, $U = \Omega\left(Y-\frac{H}{2}\right)$, $V = \Omega\left(\frac{L}{2}-X\right)$

4) Along the remainder solid boundaries,.$\partial\theta/\partial Y = U = V = 0$

The thermal field can be quantified locally and globally using the local and average Nusselt numbers along the hot surface of the cylinder as computed from the followings:

$$Nu=-\frac{k_{eff}}{k_f}\frac{\partial\theta}{\partial n} \tag{7}$$

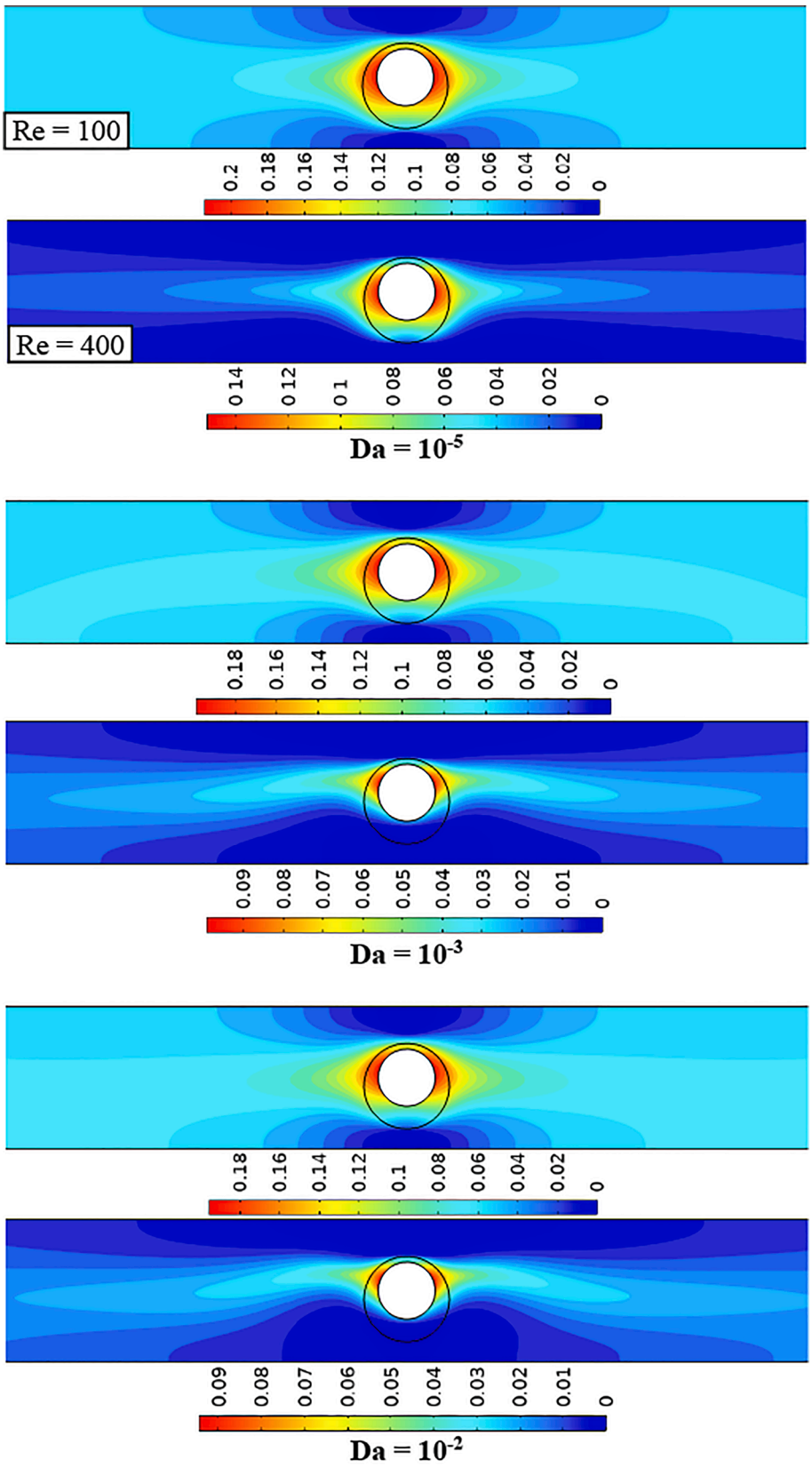

Fig. 11. Isotherms of stationary cylinder (Ω = 0) with Darcy number for Re = 100, 400 and δ/D = 0.15.

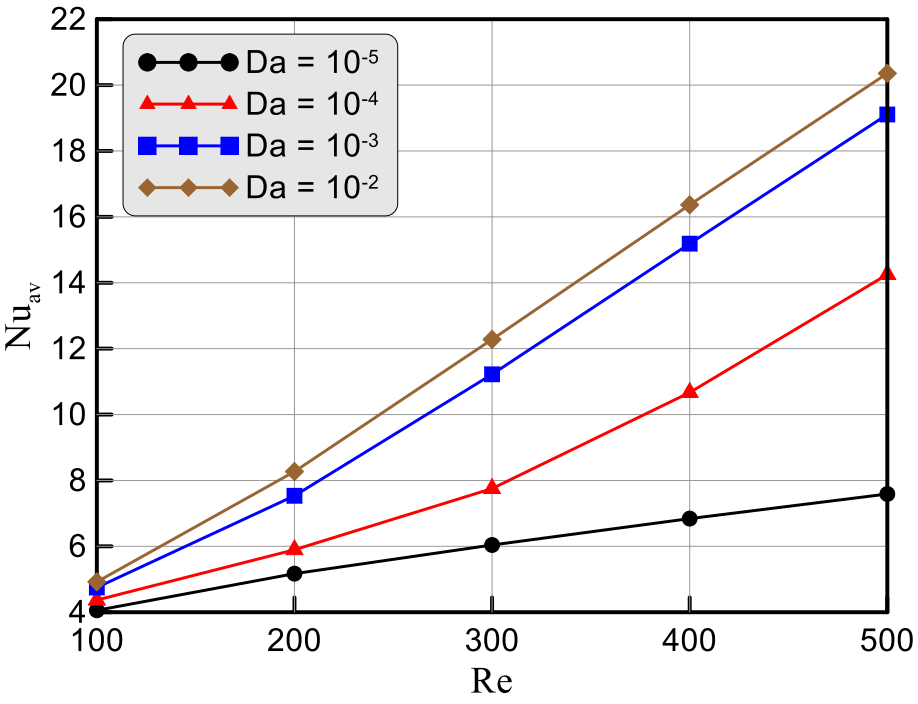

Fig. 12. Variation of Nusselt number with the Reynolds number and different Darcy number for δ/D = 0.15 and Ω = 0.

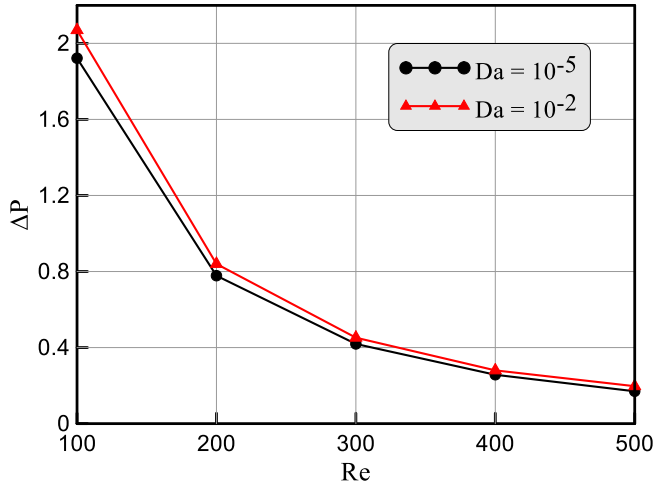

Fig. 13. Pressure drop with Re and Da for Ω = 5 and δ/D = 0.15.

$$Nu_{av} = \frac{1}{S}\int_0^S Nu \tag{8}$$

The flow field is quantified by the streamlines, which are the lines tangent to the velocity vectors and represented by $U = \frac{\partial \Psi}{\partial Y}$ and $V = -\frac{\partial \Psi}{\partial X}$.

3. Numerical solution

The domain of the problem is divided into a number of elements, and the equations (1) to (4) are discretized according to the finite element method FEM. By exploiting this method, it is possible to deal with curved and straight boundaries with high accuracy. In this method, the unknown variables are defined on the nodes of each element using basis functions. The basic functions result from interpolating the velocity, temperature and pressure by selecting a basis function $\left[\Phi_i^k\right]_i^M$ for implementing approximation solutions for these three variables.

$$\begin{aligned} U, V &\approx \sum_i^M (U, V)_i^k \Phi_i^k(X, Y), \\ \theta &\approx \sum_i^M \theta_i^k \Phi_i^k(X, Y), \\ P &\approx \sum_i^M \mathrm{P}_i^k \Phi_i^k(X, Y) \end{aligned} \tag{9}$$

the subscripts *i, k and M* represent the node number, time iteration and number of nodes, respectively.

The finite element technique (FEM) was used in this work to solve the governing equations and boundary conditions. In particular, a weak version of the governing equations was integrated across mesh elements to yield residual equations, which were then solved using a second-order algorithm. These equations were solved using the PARDISO solver [43–45]. PARDISO, which stands for Parallel Direct Solver, is a package for directly solving large sparse linear systems of equations. It leverages parallelism to solve the problems concurrently on several processors, which may drastically cut the calculation time. In addition, the coupled equations were solved using the Newton technique with a damping factor of 0.80 and a relative error criterion of less than 10^{-3}. For the sake of the stability, we implemented the second order up-wind and cross-wind stabilization schemes, which overcome the numerical instabilities arising from the convective and diffusive terms. Moreover, the cross-wind scheme obviates the numerical over and under-shooting.

The physical domains are discretized in the unstructured form to permit adaptive refining of the mesh within the steep gradients of velocity and temperature close to the surfaces of the rotating cylinder and the channel walls. To test the mesh dependency solution, several meshes were inspected for the case of Re = 400, Ω = 0, Da = 10^{-2}, and δ/D = 0.15. It is deduced from this test that the suitable mesh is composed of 141,118 elements (M4) as depicted in Table 1 and Fig. 2, which is selected as it is comparable between the accuracy and the time taken in the numerical solution. A close-up view of the M4 mesh is portrayed in Fig. 3.

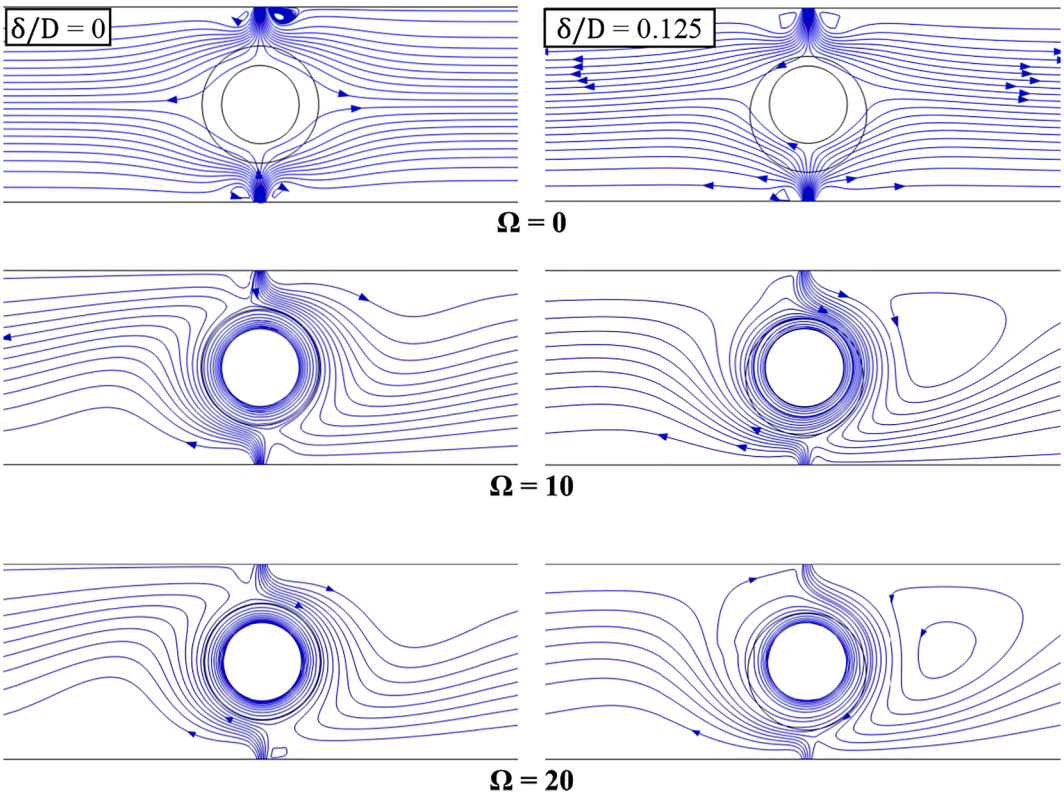

Fig. 14. Streamlines around stationary and rotating cylinder for two different rotational speeds and Re = 300 and Da = $10^{-3.}$

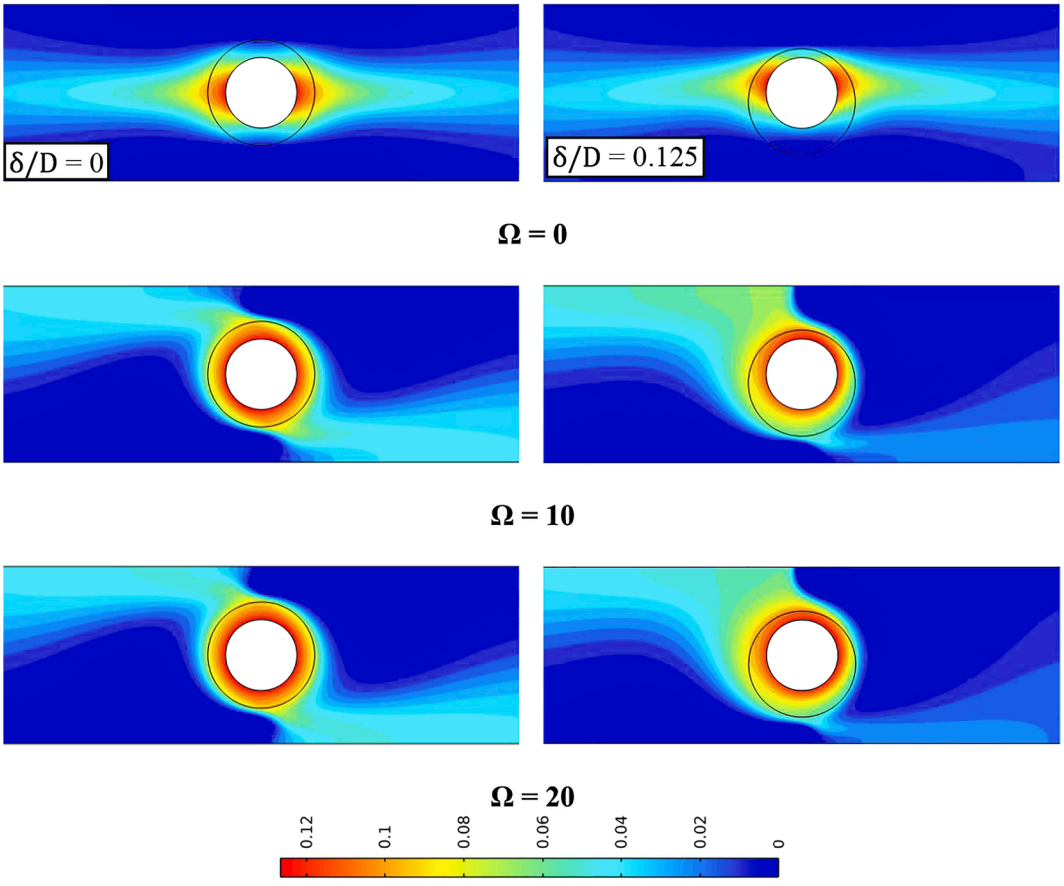

Fig. 15. Isotherms of stationary and rotating cylinder for two different rotational speeds and Re = 300 and Da = $10^{-3.}$

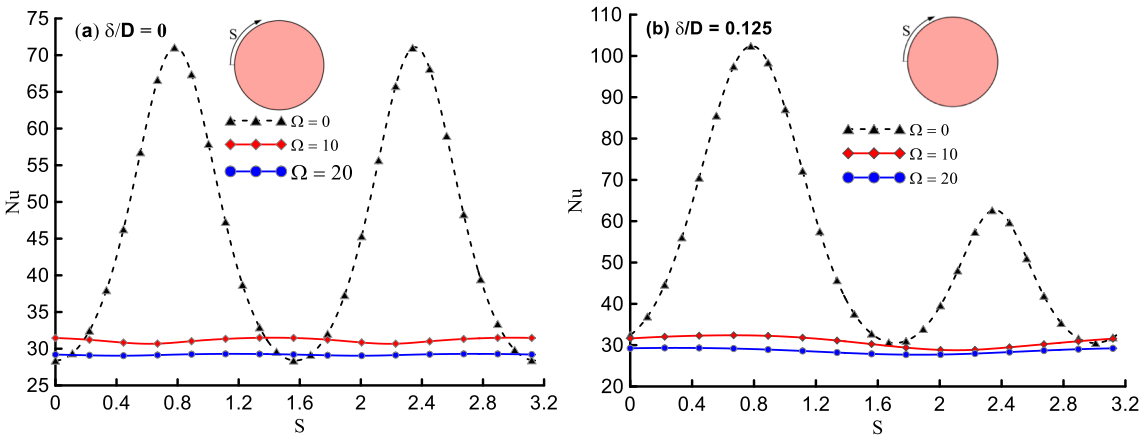

Fig. 16. Local Nusselt number for Re = 300, Da = 10^{-3} and (a) δ/D = 0, (b) δ/D = 0.125.

4. Results and discussion

4.1. Parameters and validation

The results are collected by varying the eccentricity between the porous surface layer and the cylinder by δ/D = 0 – 0.175; Darcy number by 10^{-5} – 10^{-1} to inspect the effect of the drag of the porous upon the jets; Reynolds number from 100 to 500 to inspect the ability of the jets on penetrating the porous layer and also to be within the laminar region. To inspect the effect of rotation speed, Ω was varied from 0 to 20 clockwise. The counterclockwise has not been considered because of the symmetry about a vertical line joining the centers of the two jets, cylinder and the porous surface layer. The porous surface layer is assumed to be composed of fine sandstone with thermal conductivity of k_s = 2.507 W/m.K and porosity of 0.1331 [46]. The cooling fluid is water at 24 °C; thus, Prandtl number is equal to Pr = 6.2.

To ascertain the reliability of the used numerical code, a special case of a hot cylinder ingrained in a porous medium and packed in an open-ended vertical vessel was solved. This case is one of the several experiments done by Nasr et al. [5]. The porous medium was composed of glass beads of 2.85 mm diameter, 1.01 W/m.K thermal conductivity and 0.37 porosity. The diameter of the hot cylinder was D = 12.7 mm. Al-Sumaily [47] explained that this case could be treated as a non-dimensional problem, where the domain was confined by 12D height and 10D width. The inlet boundary conditions are set as $\theta = 0$ and $V = -1$, on the cylinder $\partial\theta/\partial n = -1$, while at outlet, the pressure is set at $P = 0$. The side boundaries were set as infinity boundaries. The fluid was air, Pr = 0.7. Results of the comparison show good agreement, especially at a high Peclet number (Pe = Re * Pr), as shown in Table 2 and Fig. 4. The higher percentage errors indicated at low Peclet numbers may refer to the imperfect value of the drag coefficient C_f (Eqn. (5)) of the Darcy-Forchheimer model for low velocities. The present comparison confirms what was reported by Al-Sumaily [47], who solved the same problem using finite volume method. Table 2 presents the quantified error between the present numerical computations and the experimental results of Nasr et al. [5].

4.2. Impact of the eccentricity of the porous layer

The impact of the eccentricity is examined in the case of non-rotating cylinder (stationary cylinder, Ω = 0) and a Reynolds number Re = 300, Fig. 5 displays the streamlines for different eccentricities for two values of the Darcy numbers. The figure portrays that the jets do not penetrate into the porous layer when is relatively small (Da = 10^{-5}), even at δ/D = 0.175, i.e. when the downward jet impinges upon a very thin porous sector. This implies that the inertia of the two jets at Re = 300 is unable to overcome the drag of the porous layer. Nevertheless, for Da = 10^{-2} (low drag layer) the jets penetrate into the porous annulus for all values δ/D. The streamlines show two secondary vortices on both sides of each jet. These vortices disappear from the effective zone of the upward jet (underneath the cylinder) when δ/D = 0.175, i.e., when the portion of the porous layer facing the upward jet becomes thicker; thus, it restrains the upward jet in the early distance.

The impact of δ/D on the distribution of dimensionless temperature is presented in Fig. 6, which elucidates that the thermal boundary layers shift upward with increasing δ/D for a little drag porous layer (Da = 10^{-2}). This reveals the combined actions of water jets and the effective thermal conductivity of the porous layer, which becomes more effective in thick porous sectors as shown when δ/D = 0.175. It is worth mentioning that the asymmetric thermal boundary layer leads to higher temperature gradients resulting in cylinder subject to thermal stresses, the issue that led us to suggest the rotation of the cylinder. For δ/D = 0, the thermal boundary layer is symmetric around the hot cylinder. It can be deduced, hence, that the eccentricity can serve in widening the cold zone along the circumference of the cylinder, but since Ω = 0, the uniformity of the temperature of the surface is still absent.

In order to understand the variation of the thermal boundary layer with the eccentricity δ/D and Darcy number, the local Nusselt number *Nu* along the circumference of the hot cylinder was calculated, as depicted in Fig. 7. The figure reveals that *Nu* is maximal at the stagnation zones and for all values of δ/D. Having a concentrated look at Fig. 7 (a) for Da = 10^{-5}, it is possible to notice that the eccentricity δ/D contributes to the weakening of the local Nusselt number within the upper half of the cylinder and strengthens it along the lower half. The explanation of this trend refers to the fact that at Da = 10^{-5}, the drag of the porous surface layer restricts the motion of the fluid and hence, the role of the inertia on the local heat transfer diminishes. On the other hand, the local heat transfer depends on the thermal conductivity of the porous layer. Therefore, Nu is proportional to the quantity of the porous medium. As Da = 10^{-2} (Fig. 7 (b)), the jets meet low drag from the porous layer; therefore, the inertial of the impinging jet overcomes the gain arising from the effective thermal conductivity. Thus, the Nu is inversely proportional to the amount of the porous medium surrounding the cylinder. Comparing the scales of Fig. 7 (a) and (b), it is observed that the Nu values of Da = 10^{-2} are more than twice of Da = 10^{-5} values.

To comprehend the global effect of the δ/D with Darcy number, Fig. 8 displays a clear positive role of δ/D on the average Nusselt number Nu_{av}. The trend of increasing Nu_{av} with δ/D becomes stronger because of the combination of the freely penetrating jets into the porous layer and its effective thermal conductivity. The percentage increase of Nu_{av} when δ/D is shifted from 0 to 0.175 are 4.6%, 14% and 28% for Da = 10^{-5}, 10^{-4} and 10^{-2}, respectively.

Fig. 9 elucidates that the eccentricity elevates the drop of the dimensionless pressure (ΔP) for a rotating cylinder. This pattern is

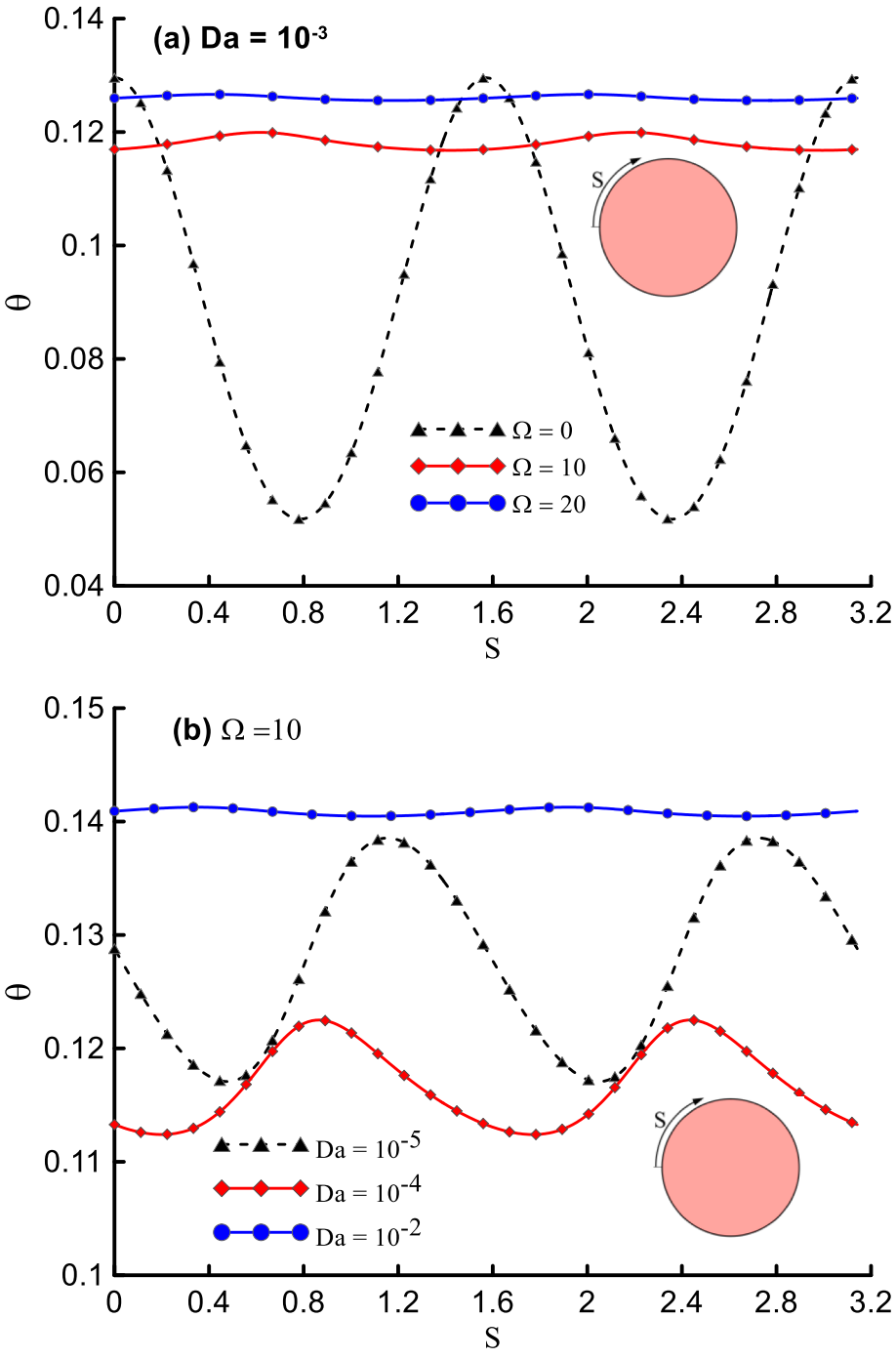

Fig. 17. Temperature distribution along the hot cylinder for Re = 300, δ/D = 0 and (a) Da = 10^{-3} and different rotational speeds, (b) Ω = 10 and different Darcy numbers.

referred to the excessive resistance of the large thickness due to the eccentric porous layer, which resists the upward jet. Whereas the variation of the pressure drop with eccentricity is marginal for non-rotating cylinder.

4.3. Impact of Darcy and Reynolds numbers

To comprehend the insight into the influence of the Darcy number, the streamlines and isotherms for low and high Reynolds number were pursued as depicted in Figs. 10 and 11. The streamlines of Fig. 10 portray that the secondary vortices formed with stronger jets (Re = 400) expand in the zone of the upward jet when Da = 10^{-2}. This can be ascribed to the separation phenomenon in the strong jet when it encounters little drag. For Da = 10^{-5}, the main-stream of the upward jet is evenly turned to cross-flow due to the considerable drag of the porous layer, thus, there is no space viable for the separation. The distribution of the isotherms in Fig. 11 indicates how the temperature drops with Darcy and Reynolds numbers. This drop in temperature is supported by the increase of the average Nusselt number, as shown in Fig. 12. This figure highlights the more pronounced role of Re with higher Da, where the percentage increase of Nu_{av} when Re increases from 100 to 500 are 87% and 314% for Da = 10^{-5} and 10^{-4}, respectively.

The drop of the dimensionless pressure with Reynolds number (Fig. 13) shows the well-known pattern of the decreasing pressure drop

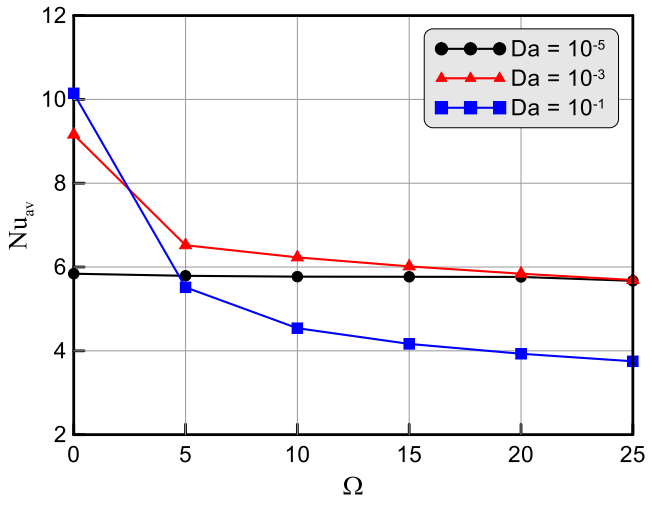

(a) δ/D = 0

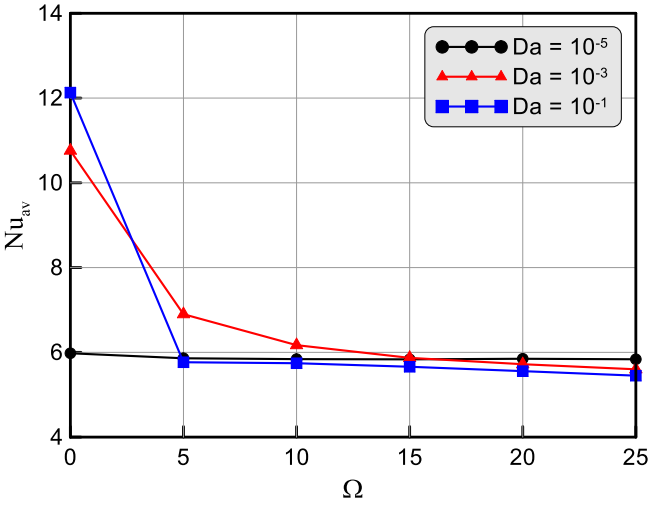

(b) δ/D = 0.125

Fig. 18. Variation of Nusselt number with the rotational speeds and different Darcy number for Re = 300 and (a) δ/D = 0, (b) δ/D = 0.125.

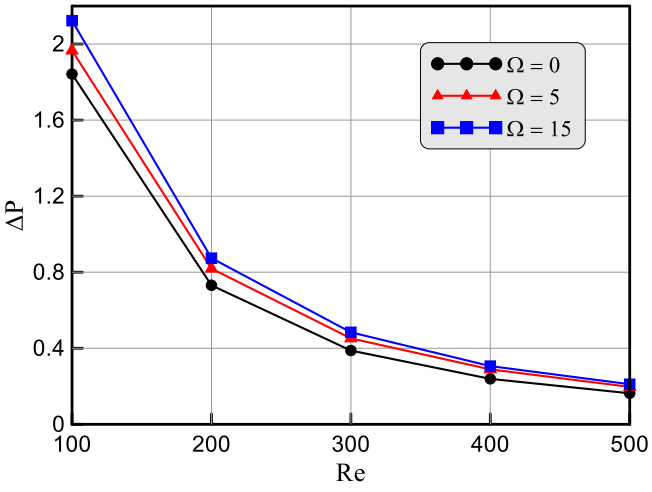

Fig. 19. Pressure drop with Re and the rotational speed for Da = 10^{-3} and δ/D = 0.15.

with Reynolds number. This is explicated by the decrease of the viscous effect at higher Reynolds number.

4.4. Impact of cylinder rotation

One of the main topics of this study is the role of rotating the hot cylinder, which is covered by the porous surface layer. This effect is illustrated in Fig. 14 for concentric and eccentric layers. The figures disclose an important topic, that is, the cross-flow is disturbed evenly on both outlets for the concentric layer, while in the eccentric case, the downward jet is guided by the rotating cylinder due to the shorter path in a low drag zone. This process is mainly caused by the friction effect. Most of the guided stream is brought to encounter the upward jet and then turns to the left cross-flow, leading to asymmetric outlet flows. Moreover, a secondary vortex on the right of the annulus blocks the channel leading to pushing most of the fluid towards the left outlet. This scenario of cross-flow makes the water leaving the left outlet hotter than other zones, as depicted in Fig. 15 for eccentric annulus.

To inspect the thermal field closely, the distribution of the Nu with the rotational speed Ω is exhibited in Fig. 16. For an eccentric layer (Fig. 16 (a)), the symmetric oscillation of Nu decreases and flattens strongly when Ω increases to a non-zero value. The same effect is noticed with the eccentric layer (Fig. 16 (b)), but with asymmetric distribution of Nu at Ω = 0 because of the eccentricity of the porous layer. However, with a rotating cylinder, the distribution flattens vastly due to the steep reduction of Nu. It can be deduced from the figure that the rotation of the cylinder serves to uniform the boundary layer along the circumferential path of the cylinder, but it deviates the impinging jets and leads to scattering the stagnation zones, thus weakening the local Nusselt number. The uniformity of the boundary layer around the rotating cylinder means that the surface temperature of the cylinder becomes uniform. This can be observed in Fig. 17 (a), which implies the uniformity of the surface temperature with non-zero values of Ω. This uniformity of the temperature is one of the main demands in steel production to avoid surface thermal stresses. However, pumping more fluid through the jets can compensate for the concomitant increase of temperature with Ω. Fig. 17 (b) discovers that the role of rotation in temperature uniformity is more pronounced in a porous medium of high permeability, i.e., high Darcy number. The global impact of the rotation is presented in Fig. 18, where the average Nusselt number declines with Ω in concentric (Fig. 18 (a)) and eccentric (Fig. 18 (b)) porous layers. This is because, as mentioned above, due to the deviation of the two jets when they approach the rotating cylinder. This explanation is demonstrated by having a glance at the Nu_{av} of Da = 10^{-5}. It is uninfluenced by Ω because the inertia of the jet dissipates in the porous layer before they reach the rotating cylinder. The reduction in Nu_{av} at 10^{-3} when Ω varies from 0 to 25 is 38% for δ/D = 0 and 48% for δ/D = 0.125.

Fig. 19 depicts an increase in the pressure drop with increasing the rotational speed of the cylinder. The boosted frictional effect between the impinging jet and the rotating surface is behind this pattern.

4.5. Demonstration of the benefit of the porous surface layer

In order to examine the role of the porous surface layer, the bared cylinder is compared with another covered by a porous surface of Da = 10^{-3} and δ/D = 0 for Ω = 0 and 10. The results of this comparison are plotted in Figs. 20 – 23. The rotation affects the streamlines of the bared cylinder greater than the covered cylinder, as can be seen in Fig. 20. In the bared cylinder, two big vortices circulate on the sides of the cylinder. These vortices prevent the rotating heated water from discharging to outlets. While for covered cylinders, substantial zones of heated water leaving the channel are observed (Fig. 21). More precisely, Figs. 22 and 23 demonstrate the positive job of the porous surface layer in both still and rotating cylinders on the Nu_{av}. This job becomes more effective with increasing Da number. Nevertheless, the lower Darcy number produces an adverse action on Nu_{av}, as shown in Fig. 23 for Da = 10^{-5}. However,

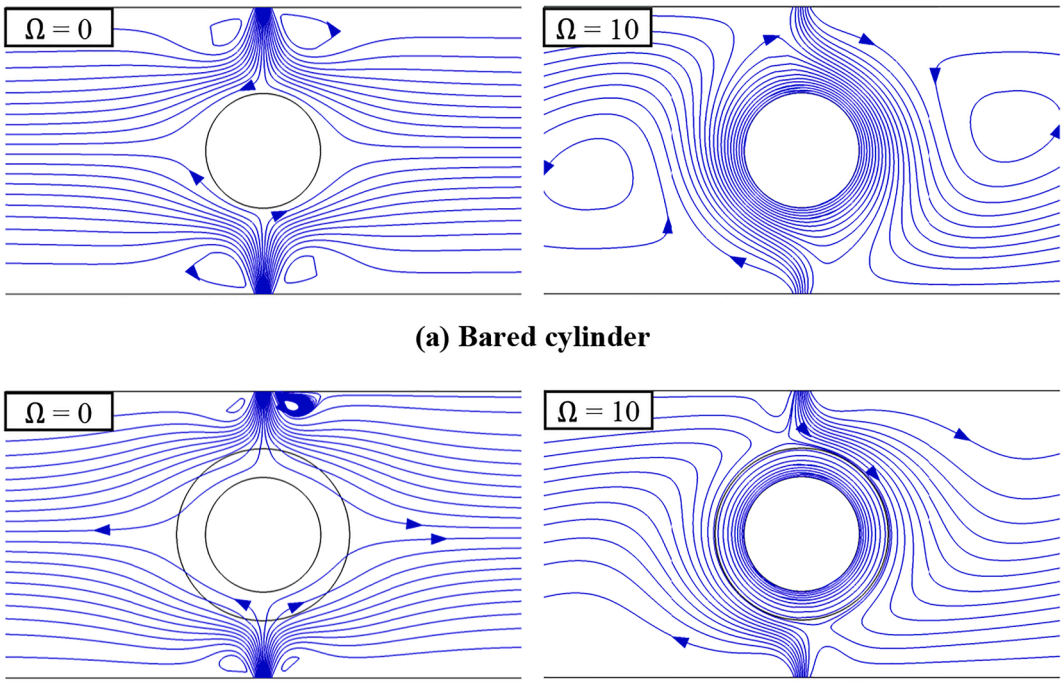

Fig. 20. Streamlines around bared and covered cylinders for Re = 100.

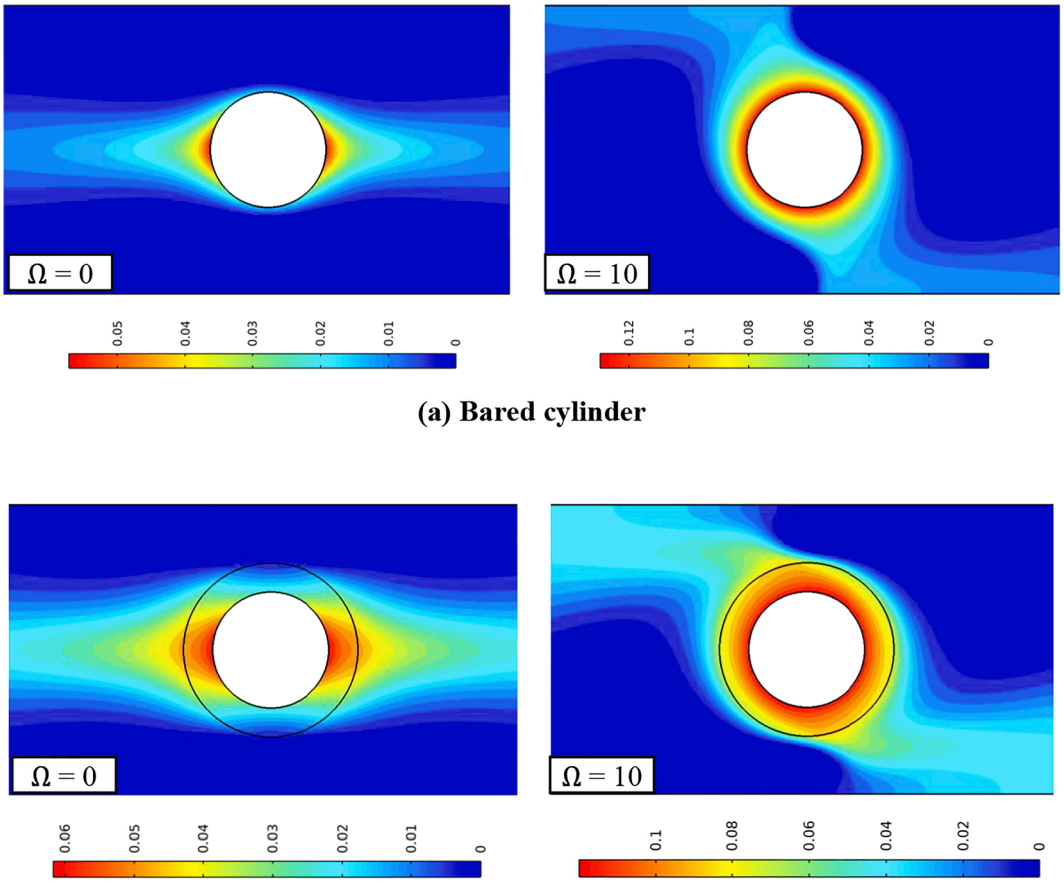

Fig. 21. Isotherms around bared and covered cylinders for Re = 100.

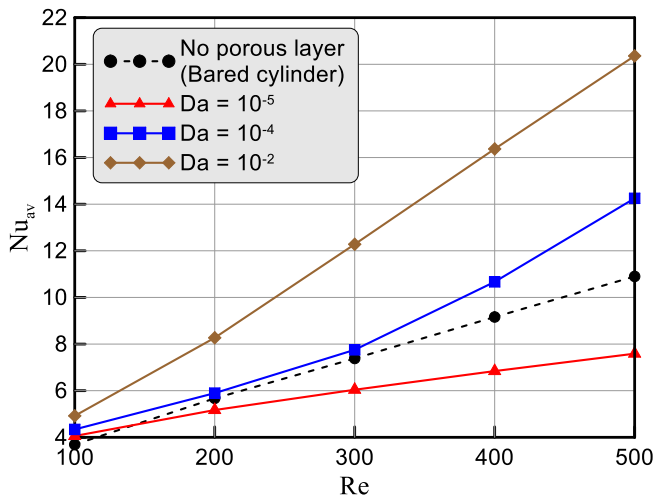

Fig. 22. The role of the porous layer on the Nusselt number for Ω = 0 and δ/D = 0.03.

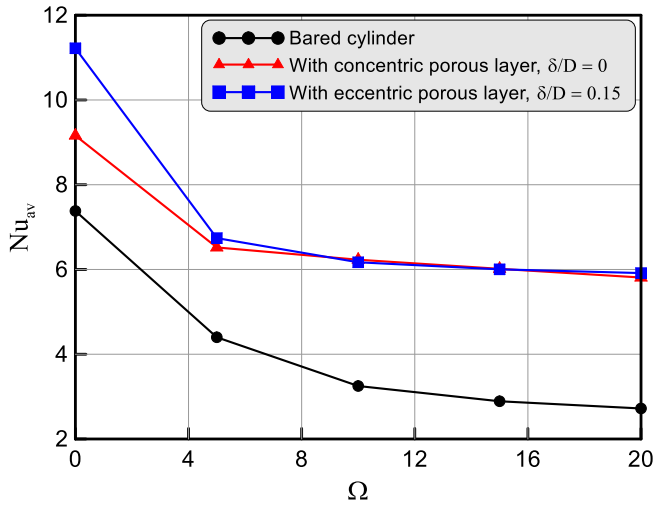

Fig. 23. The role of the porous layer on the Nusselt number for Re = 300 and Da = 10^{-3}.

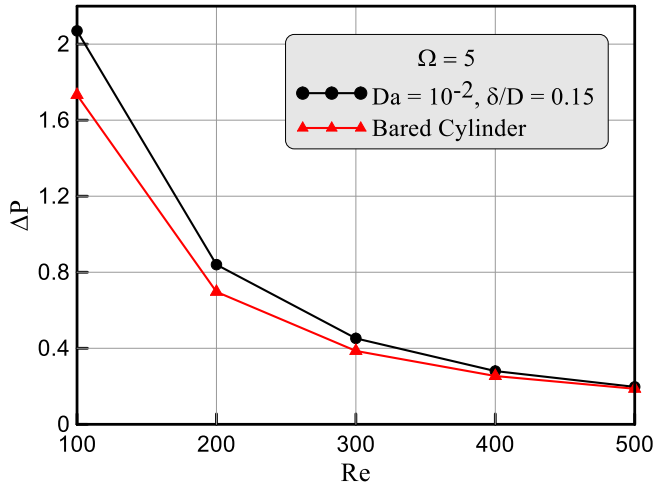

Fig. 24. Effect of the porous layer on the pressure drop.

at Re = 400, Ω = 0 and δ/D = 0.15, the Nu_{av} increases by 78% when the cylinder is covered by a porous layer of Da = 10^{-2} and decreases by 25% when Da = 10^{-5}. Contrarily, the porous layer causes a pressure drop higher than that of the Bared cylinder as presented in Fig. 24. This is obviously exemplified by the added drag coefficient existing in the Darcy-Forchheimer model (Eqns. (2) and (3)). Howsoever, the effect of the porous layer on the pressure drop vanishes at higher Reynolds number.

5. Summary and conclusions

This paper has given an account to the idea of covering a rotating hot cylinder with an eccentric porous layer undergoing two upward and downward impinging jets. The problem is solved numerically and the used numerical method has been confirmed with experimental data. In this study, comparisons between the bared and covered cylinder and between the still and rotating cylinder were achieved. This problem is encountered in steel production and how to avoid thermal stresses. In summary, the conclusions drawn from our results are;

i) The existence of the porous surface layer augments the average Nusselt number if the Darcy number of this porous layer is large enough. For instance, at Re = 400 and stationary cylinder, the average Nusselt number of the covered cylinder is larger than the bared cylinder by 78% when Darcy number is 10^{-2} and lower than the bared cylinder by 25% when Darcy = 10^{-5}.
ii) Globally, the eccentricity of the porous layer provides a positive role in augmenting the average Nusselt number, but it elevates the pressure drop. At Re = 300, increasing the eccentricity from 0 to 0.175 enhances the Nusselt number by 28% when Da = 10^{-2}.
iii) The rotation of the cylinder plays two roles, it brings the surface temperature of the hot cylinder uniform; and diverts the impinging jets, which in turn declines the Nusselt number. The reduction in the average Nusselt number when the rotation is raised to 25 is about 38 % and 48% for concentric and eccentric porous surface layers, respectively. The pressure drop increases with the rotation.
iv) For non-rotating cylinders, the maximal local Nusselt numbers are recorded in the stagnation zones.
v) For the low Darcy number, the local Nusselt number is proportional to the size of the porous zone, while for the high Darcy number, the local Nusselt number is inversely proportional to the size of the porous zone.
vi) As such, the optimum parameters that removes the thermal stresses from the cylinder is its rotational speed, but it declines the heat transfer. The heat transfer can be enhanced practically by immersing the rotating cylinder in a porous layer with a non-dimensional permeability of about Da = 10^{-3}.

Declaration of Competing Interest

The authors declare that they have no known competing financial interests or personal relationships that could have appeared to influence the work reported in this paper.

Data availability

Data will be made available on request.

Acknowledgements

The authors would like to thank the Deanship of Scientific Research at Umm Al-Qura University for supporting this work by Grant Code: (23UQU4310414DSR001). This research of Mohammad Ghalambaz was supported by the Tomsk State University Development Program (Priority-2030). The corresponding author (Muneer A. Ismael) extends his

thanks to University of Warith Al-Anbiyaa, Iraq for financial support for this study.

References

[1] M. Pohanka, P. Kotrbáček, Design of Cooling units for heat treatment, in: F. Czerwinski (Ed.), Heat Treatment-Conventional and Novel Applications InTech, Croatia, 2012, pp. 1–22, https://doi.org/10.5772/50492.

[2] T.G. Digges, S.J. Rosenberg, G.W. Geil, Heat treatment and properties of iron and steel, National Bureau of Standards Gaithersburg Md (1966).

[3] L. Shi, X. Zhu, Z. Du, Study on convective heat transfer characteristics of inclined jet impinging cylindrical target surface in the confined space, Appl. Therm. Eng. 218 (2023) 119316, https://doi.org/10.1016/j.applthermaleng.2022.119316.

[4] J.Z. Zhang, X.M. Tan, B. Liu, X.D. Zhu, Investigation for convective heat transfer on grinding work-piece surface subjected to an impinging jet, Appl. Therm. Eng. 51 (2013) 653–661, https://doi.org/10.1016/j.applthermaleng.2012.10.011.

[5] K. Nasr, S. Ramadhyani, R. Viskanta, An experimental investigation on forced convection heat transfer from a cylinder embedded in a packed bed, J. Heat Transf. 116 (1994) 73–80, https://doi.org/10.1115/1.2910886.

[6] M. Layeghi, A. Nouri-Borujerdi, Darcy model for the study of the fluid flow and heat transfer around a cylinder embedded in porous media, Int. J. Comput. Methods Eng. Sci. Mech., 7 (2006) 323–329, https://doi.org/10.1080/15502280600826340.

[7] G.F. Al-Sumaily, J. Sheridan, M.C. Thompson, Analysis of forced convection heat transfer from a circular cylinder embedded in a porous medium, Int. J. Therm. Sci. 51 (2012) 121–131, https://doi.org/10.1016/j.ijthermalsci.2011.08.018.

[8] H.O. Sayehvand, K.E. Dehkordi, P.A. Basiri, Numerical analysis of forced convection heat transfer from two tandem circular cylinders embedded in a porous medium, Therm. Sci. 21 (2017) 2117–2128, https://doi.org/10.2298/TSCI150307081S.

[9] K. Al-Salem, H.F. Oztop, S. Kiwan, Effects of porosity and thickness of porous sheets on heat transfer enhancement in a cross flow over heated cylinder, Int. Commun. Heat Mass transf. 38 (2011) 1279–1282, https://doi.org/10.1016/j.icheatmasstransfer.2011.07.006.

[10] S. Rashidi, A. Tamayol, M.S. Valipour, N. Shokri, Fluid flow and forced convection heat transfer around a solid cylinder wrapped with a porous ring, Int. J. Heat Mass Transf. 63 (2013) 91–100, https://doi.org/10.1016/j.ijheatmasstransfer.2013.03.006.

[11] S. Tumse, H. Zontul, H. Hamzah, B. Sahin, Numerical Investigation of Magnetohydrodynamic Forced Convection and Entropy Production of Ferrofluid around a Confined Cylinder Using Wire Magnetic Sources, Arab. J. Sci. Eng. (2022) 1–30, https://doi.org/10.1007/s13369-022-07470-5.

[12] H. Naito, K. Fukagata, Numerical simulation of flow around a circular cylinder having porous surface, Phys. Fluids 24 (2012) 117102, https://doi.org/10.1063/1.4767534.

[13] S. Sadeghipour, S.A.S. Ali, X. Liu, M. Azarpeyvand, G.R. Thorpe, Control of flows around bluff bodies mediated by porous materials, Exp. Therm. Fluid Sci. 114 (2020) 110048, https://doi.org/10.1016/j.expthermflusci.2020.110048.

[14] S.A. Showkat Ali, X. Liu, M. Azarpeyvand, Bluff body flow and noise control using porous media, In 22nd AIAA/CEAS aeroacoustics conference (2016), 2754, https://doi.org/10.2514/6.2016-2754.

[15] H. Liu, J. Wei, Z. Qu, Prediction of aerodynamic noise reduction by using open-cell metal foam, J. Sound Vib. 331 (2012) 1483–1497, https://doi.org/10.1016/j.jsv.2011.11.016.

[16] M. Farzad, H. El Ferouali, O. Kahraman, J. Yagoobi, Enhancement of heat transfer and product quality using jet reattachment nozzles in drying of food products, Drying Technol. 40 (2022) 352–370, https://doi.org/10.1080/07373937.2020.1804927.

[17] W.S. Fu, H.C. Huang, Thermal performances of different shape porous blocks under an impinging jet, Int. J. Heat Mass Transf. 40 (1997) 2261–2272, https://doi.org/10.1016/S0017-9310(96)00320-1.

[18] W. Chen, J. Cheng, A numerical analysis on the heat transfer of jet impingement with nanofluid on a concave surface covered with metal porous block, Heat Mass Transf. 56 (2020) 3071–3083, https://doi.org/10.1007/s00231-020-02902-0.

[19] C. Fischer, M.J. de Lemos, A turbulent impinging jet on a plate covered with a porous layer, Numer. Heat Transf. A: Appl. 58 (2010) 429–456, https://doi.org/10.1080/10407782.2010.508434.

[20] K. Choo, T.Y. Kang, S.J. Kim, The effect of inclination on impinging jets at small nozzle-to-plate spacing, Int. J. Heat Mass Transf. 55 (2012) 3327–3334, https://doi.org/10.1016/j.ijheatmasstransfer.2012.02.062.

[21] F. Bentarzi, A. Mataoui, M. Rebay, Effect of inclination of twin impinging turbulent jets on flow and heat transfer characteristics, Int. J. Therm. Sci. 137 (2019) 490–499, https://doi.org/10.1016/j.ijthermalsci.2018.12.021.

[22] D. Benmouhoub, A. Mataoui, Heat transfer control of an impinging inclined slot jets on a moving wall, Heat Transf.—Asian Res. 44 (2015) 568–584, https://doi.org/10.1002/htj.21138.

[23] H. Chattopadhyay, S.K. Saha, Numerical investigations of heat transfer over a moving surface due to impinging knife-jets, Numer. Heat Transf. A: Appl. 39 (2001) 531–549, https://doi.org/10.1080/10407780118047.

[24] A.K. Sharma, S.K. Sahu, The thermal and rewetting behavior of hot moving surface by water jet impingement, Appl. Therm. Eng. 159 (2019) 113950, https://doi.org/10.1016/j.applthermaleng.2019.113950.

[25] W.C. Lai, P. Yin, Y.H. Liu, Investigation of flow characteristics from an inclined jet on a heated rotating disk, Int. J. Heat Mass Transf. 127 (2018) 943–956, https://doi.org/10.1016/j.ijheatmasstransfer.2018.08.028.

[26] P. Dutta, H. Chattopadhyay, Numerical analysis of transport phenomena under turbulent annular impinging jet, Comput. Therm. Sci.: Int. Journal 13 (2021) 1–19, https://doi.org/10.1615/ComputThermalScien.2020035055.

[27] S.M. Hosseinalipour, S. Rashidzadeh, M. Moghimi, K. Esmailpour, Numerical study of laminar pulsed impinging jet on the metallic foam blocks using the local thermal non-equilibrium model, J. Therm. Anal. Calorim. 141 (2020) 1859–1874, https://doi.org/10.1007/s10973-019-09225-1.

[28] D. Singh, B. Premachandran, S. Kohli, Numerical simulation of the jet impingement cooling of a circular cylinder, Numer. Heat Transf. A: Applications 64 (2013) 153–185, https://doi.org/10.1080/10407782.2013.772869.

[29] S. Devynck, M. Gradeck, J.P. Bellot, S. Denis, M. Varlez, T. Benard, Cooling of a rotating cylinder by a subcooled planar jet-Influence of the surface velocity on boiling regime, Key Eng. Mater. 504 (2012) 1049–1054, https://doi.org/10.4028/www.scientific.net/KEM.504-506.1049.

[30] M. Gradeck, A. Kouachi, J.L. Borean, P. Gardin, M. Lebouché, Heat transfer from a hot moving cylinder impinged by a planar subcooled water jet, Int. J. Heat Mass Transf. 54 (2011) 5527–5539, https://doi.org/10.1016/j.ijheatmasstransfer.2011.07.038.

[31] S.A. Nada, Slot/slots air jet impinging cooling of a cylinder for different jets–cylinder configurations, Heat Mass Transf. 43 (2006) 135–148, https://doi.org/10.1007/s00231-006-0100-3.

[32] D. Singh, B. Premachandran, S. Kohli, Circular air jet impingement cooling of a circular cylinder with flow confinement, Int. J. Heat Mass Transf. 91 (2015) 969–989, https://doi.org/10.1016/j.ijheatmasstransfer.2015.08.037.

[33] D. Singh, B. Premachandran, S. Kohli, Double circular air jet impingement cooling of a heated circular cylinder, Int. J. Heat Mass Transf. 109 (2017) 619–646, https://doi.org/10.1016/j.ijheatmasstransfer.2017.02.035.

[34] S. Pachpute, B. Premachandran, Slot air jet impingement cooling over a heated circular cylinder with and without a flow confinement, Appl. Therm. Eng. 132 (2018) 352–367, https://doi.org/10.1016/j.applthermaleng.2017.12.091.

[35] R. Alizadeh, A.B. Rahimi, N. Karimi, A. Alizadeh, On the hydrodynamics and heat convection of an impinging external flow upon a cylinder with transpiration and embedded in a porous medium, Transport Porous Med. 120 (2017) 579–604, https://doi.org/10.1007/s11242-017-0942-9.

[36] M. Jahedi, B. Moshfegh, Experimental study of quenching process on a rotating hollow cylinder by one row of impinging jets, In 9th World Conference on Experimental Heat Transfer, Fluid Mechanics and Thermodynamics, (2017), Iguazu Falls, Brazil.

[37] T.M. Jeng, S.C. Tzeng, R. Xu, Heat transfer characteristics of a rotating cylinder with a lateral air impinging jet, Int. J. Heat Mass Transf. 70 (2014) 235–249, https://doi.org/10.1016/j.ijheatmasstransfer.2013.10.069.

[38] H. Ma, W. Zhou, X. Lu, Z. Ding, Y. Cao, N. Deng, Y. Zhang, Investigation on the air flow and heat transfer from a horizontal rotating cylinder, Int. J. Therm. Sci. 95 (2015) 21–28, https://doi.org/10.1016/j.ijthermalsci.2015.03.017.

[39] M.A. Bijarchi, A. Eghtesad, H. Afshin, M.B. Shafii, Obtaining uniform cooling on a hot surface by a novel swinging slot impinging jet, Appl. Therm. Eng. 150 (2019) 781–790, https://doi.org/10.1016/j.applthermaleng.2019.01.037.

[40] Y. Li, B. Li, F. Qi, S.C. Cheung, Flow and heat transfer of parallel multiple jets obliquely impinging on a flat surface, Appl. Therm. Eng. 133 (2018) 588–603, https://doi.org/10.1016/j.applthermaleng.2018.01.064.

[41] S.H. Kim, H.D. Kim, K.C. Kim, Measurement of two-dimensional heat transfer and flow characteristics of an impinging sweeping jet, Int. J. Heat Mass Transfer 136 (2019) 415–426, https://doi.org/10.1016/j.ijheatmasstransfer.2019.03.021.

[42] D.A. Nield, A. Bejan, Convection in Porous Media, (Fourth ed.), New York: springer, 2013, https://doi.org/10.1007/978-1-4614-5541-7.

[43] O. Schenk, K. Gärtner, Solving unsymmetric sparse systems of linear equations with PARDISO, Futur. Gener. Comput. Syst. 20 (3) (2004) 475–487.

[44] P. Wriggers, Nonlinear Finite Element Methods, Springer Science & Business Media, 2008.

[45] F. Verbosio, A. De Coninck, D. Kourounis, O. Schenk, Enhancing the scalability of selected inversion factorization algorithms in genomic prediction, J. Comput. Sci. 22 (2017) 99–108.

[46] W. Zhu, X. Su, Q. Liu, Analysis of the relationships between the thermophysical properties of rocks in the Dandong Area of China, Eur. J. Remote Sens. 54 (2021) 122–131, https://doi.org/10.1080/22797254.2020.1763205.

[47] G.F.S. Al-Sumaily, Convection heat transfer from cylinders in a porous medium using the two-equation energy model, 2013, (Doctoral dissertation, Monash University), https://doi.org/10.4225/03/589bc4e463a12.